Sexual pheromone modulates the frequency of cytosolic Ca²⁺ bursts in *Saccharomyces cerevisiae*

Natalia Carbó[a,†], Nahuel Tarkowski[b,†], Emiliano Perez Ipiña[c], Silvina Ponce Dawson[c], and Pablo S. Aguilar[a,b,*]

[a]Laboratorio de Biología Celular de Membranas, Institut Pasteur de Montevideo, Montevideo, Uruguay; [b]Laboratorio de Biología Celular de Membranas, Instituto de Investigaciones Biotecnológicas, Universidad de San Martin, Buenos Aires, Argentina; [c]Departamento de Física and IFIBA, CONICET, Facultad de Ciencias Exactas y Naturales, Universidad de Buenos Aires, Buenos Aires, Argentina

[AQ 1]

ABSTRACT Transient and highly regulated elevations of cytosolic Ca²⁺ control a variety of cellular processes. Bulk measurements using radioactive Ca²⁺ and the luminescent sensor aequorin have shown that in response to pheromone, budding yeast cells undergo a rise of cytosolic Ca²⁺ that is mediated by two import systems composed of the Mid1-Cch1-Ecm7 protein complex and the Fig1 protein. Although this response has been widely studied, there is no treatment of Ca²⁺ dynamics at the single-cell level. Here, using protein calcium indicators, we show that both vegetative and pheromone-treated yeast cells exhibit discrete and asynchronous Ca²⁺ bursts. Most bursts reach maximal amplitude in 1–10 s, range between 7 and 30 s, and decay in a way that fits a single-exponential model. In vegetative cells, bursts are scarce but preferentially occur when cells are transitioning G1 and S phases. On pheromone presence, Ca²⁺ burst occurrence increases dramatically, persisting during cell growth polarization. Pheromone concentration modulates burst frequency in a mechanism that depends on Mid1, Fig1, and a third, unidentified, import system. We also show that the calcineurin-responsive transcription factor Crz1 undergoes nuclear localization bursts during the pheromone response.

INTRODUCTION

Calcium (Ca²⁺) signals are pervasive in eukaryotic cells, where this divalent cation acts as a messenger that rapidly modifies protein electrostatic charge, shape, and function. Fast and transient elevations of free cytosolic Ca²⁺ levels control a wide variety of cellular processes and adaptive responses. The versatility of Ca²⁺ signaling systems is reflected in the very different spatial and temporal distributions that the Ca²⁺ concentration can display. Some cellular processes, such as Ca²⁺-triggered exocytosis, are executed in milliseconds within a very localized subcellular environment. Other

processes, such as developmental programs and gene transcription control, require longer Ca²⁺ transients (minutes to hours) that, in multicellular organisms, might even be propagated throughout an entire tissue. This diversity can be captured by live imaging of Ca²⁺ dynamics, enabling systematic analysis of cell and tissue behavior in response to a changing environment.

In *Saccharomyces cerevisiae*, cytosolic Ca²⁺ signals are implicated in the response to several environmental challenges, including osmotic imbalance (Batiza *et al.*, 1996; Denis and Cyert, 2002), the presence of mating pheromone (Ohsumi and Anraku, 1985; Iida *et al.*, 1990), protein misfolding (Bonilla *et al.*, 2002), high pH (Viladevall *et al.*, 2004), and glucose addition under starvation (Nakajima-Shimada *et al.*, 1991). There is a vast body of knowledge on the transporters, sensors, and effectors implicated in *S. cerevisiae* Ca²⁺ homeostasis (for recent reviews, see Cunningham, 2011; Cyert and Philpott, 2013). Of note, our understanding of Ca²⁺ dynamics in yeast relies on bulk monitoring of cellular Ca²⁺ levels using either radioactive ⁴⁵Ca²⁺ or the bioluminescent sensor aequorin. Unlike research on mammalian cells, single-cell monitoring of Ca²⁺ signals is almost unreported in *S. cerevisiae* (Cunningham, 2011). Here we address this issue by adapting a fluorescent protein Ca²⁺

sensor to budding yeast and exploring single-cell Ca^{2+} dynamics during the pheromone response.

S. cerevisiae has two sexes or mating types, *MAT**a*** and *MATα*. Haploid cells secrete a mating type–specific pheromone that is sensed by cells of the complementary mating type. Pheromone binding to its cognate receptor triggers a canonical mitogen-activated protein (MAP) kinase signaling cascade that leads to cell cycle arrest, transcriptional reprogramming, and polarized growth toward the mating partner. Pioneering work using $^{45}Ca^{2+}$ showed that haploid yeast cells treated with mating pheromone take up extracellular Ca^{2+} in a dose-dependent manner (Ohsumi and Anraku, 1985). The $^{45}Ca^{2+}$ uptake begins 30–40 min after pheromone addition and is sustained over an additional 60–80 min, being coincident with active polarized growth and formation of a cell shape called shmoo (Ohsumi and Anraku, 1985). Bulk Ca^{2+} monitoring using the bioluminescent sensor aequorin showed a similar timing in cytosolic Ca^{2+} level changes during the pheromone response (Nakajima-Shimada *et al.*, 1991; Muller *et al.*, 2003). Pheromone-induced Ca^{2+} uptake depends on at least two plasma membrane transporting systems, the high- and low-affinity calcium import systems (HACS and LACS, respectively). HACS depends on the simultaneous presence of three plasma membrane proteins: Cch1, a homologue of the catalytic α-subunit of voltage-gated Ca^{2+} channels (Fischer *et al.*, 1997; Paidhungat and Garrett, 1997; Muller *et al.*, 2001); Mid1, an integral membrane glycoprotein that physically interacts with Cch1 (Iida *et al.*, 1994; Locke *et al.*, 2000); and Ecm7, a predicted tetraspanning membrane protein with similarity to the catalytic γ-subunit of voltage-gated Ca^{2+} channels (Martin *et al.*, 2011). Cch1, Mid1, and Ecm7 proteins are constitutively expressed, but HACS activity is very low in vegetative growing cells, presumably due to negative feedback regulation mediated by the Ca^{2+}/calmodulin-activated phosphatase calcineurin (CN; Locke *et al.*, 2000; Muller *et al.*, 2001). LACS requires the presence of Fig1, a pheromone-induced plasma membrane protein. Like Ecm7, Fig1 has four predicted transmembrane domains with structural resemblance to the transmembrane domains of claudins and the γ-subunit of voltage-gated Ca^{2+} channels (Muller *et al.*, 2003). Here we show that the increase of cytosolic Ca^{2+} during response to the pheromone is not continuous but is composed of a series of discrete Ca^{2+} bursts that are more frequent as pheromone concentration increases. This pheromone-dependent increase of Ca^{2+} burst frequency depends on HACS, LACS, and a third, unidentified Ca^{2+} transport system. In parallel with the cytosolic Ca^{2+} bursts, the CN-responsive transcription factor Crz1 undergoes nuclear localization bursts in response to pheromone.

RESULTS AND DISCUSSION
Extracellular Ca^{2+} stress evokes rapid changes in fluorescence of GCaMP in yeast
To monitor cytosolic Ca^{2+} ($[Ca^{2+}]_{cyt}$) signals in *S. cerevisiae*, we adapted different versions of the green fluorescent protein (GFP)–calmodulin fusion protein (GCaMP) Ca^{2+} indicators originally developed to follow neuronal activity. We built strains bearing Ca^{2+} indicator genes GCaMP3 (Tian *et al.*, 2009) and GCaMP6f (Chen *et al.*, 2013) stably inserted in a single copy in the *URA3* locus (*Materials and Methods*). Growth rate measurements in different conditions indicated that neither GCaMP3 nor GCaMP6f interfered with *S. cerevisiae* cell growth in standard culture conditions (*Materials and Methods*). In vivo responses for both Ca^{2+} reporters were evaluated by live fluorescence microscopy monitoring of cells subjected to calcium stress. Inspection of short (10–13 min) time-lapse movies revealed that cells growing in standard synthetic

medium show low levels of cytosolic fluorescence and sporadically exhibit transient increases of fluorescence. These observations are consistent with previously reported bulk measurements of $[Ca^{2+}]_{cyt}$ levels showing that mid logarithmic–growing cells incubated in standard medium keep low $[Ca^{2+}]_{cyt}$ and low CN activity and do not actively accumulate extracellular calcium (Ohsumi and Anraku, 1985; Stathopoulos and Cyert, 1997; Muller *et al.*, 2003). However, soon after the addition of calcium, numerous cells showed high cytosolic fluorescence levels, strongly suggesting that both indicators are functional in *S. cerevisiae* (Figure 1A). Cell segmentation of time-lapse images and quantitation of normalized fluorescence levels ($\Delta F/F_0$; see *Materials and Methods*) confirmed that both GCaMP3 and GCaMP6f are responsive to Ca^{2+} stress in *S. cerevisiae*, as suspected (Figure 1B). Single-cell $\Delta F/F_0$ traces were then used to compare the performance of both GCaMP variants in terms of registered maximum amplitudes and signal-to-noise ratios (SNRs; Figure 1, C and D). In contrast with tests in cultured neurons and animal models, in which GCaMP6f clearly outperformed GCaMP3 (Chen *et al.*, 2013), the two indicators exhibited similar performances in budding yeast. Both GCaMP3 and GCaMP6f outperformed yellow Cameleon YC2.12, a Förster resonance energy transfer–based calcium sensor that exhibited very low SNR in *S. cerevisiae* cells (Cai *et al.*, 2008). Unlike the calcium dye fura-2, which, after loading rapidly, accumulates in yeast vacuoles (Iida *et al.*, 1990), GCaMP3 and GCaMP6f are stable cytosolic proteins enabling long-term monitoring of $[Ca^{2+}]_{cyt}$ dynamics. Given that GCaMP3 and GCaMP6f behaved similarly, we decided to use GCaMP6f for the experiments because it has been further optimized for fast Ca^{2+} imaging (Chen *et al.*, 2013).

High-speed monitoring of $[Ca^{2+}]_{cyt}$ in single cells responding to α-factor
Having successfully adapted two GCaMP indicators to *S. cerevisiae*, we proceeded to characterize single-cell $[Ca^{2+}]_{cyt}$ dynamics during the pheromone response. Aequorin luminescence monitoring of $[Ca^{2+}]_{cyt}$ indicated that, after a lag of 40 min, pheromone-treated cells experienced a slow increase of $[Ca^{2+}]_{cyt}$ that peaked after 30 min and then needed an additional ~60 min to decline to basal levels (Muller *et al.*, 2003). Because calcium-stress results indicated that $[Ca^{2+}]_{cyt}$ fluctuations were on the order of seconds to minutes (Figure 1), we first imaged pheromone-treated cells at high speeds (e.g., 5 frames/s). *MAT**a*** GCaMP6f cells were grown to mid log phase and treated with α-factor, and then, at different time points (10–80 min after pheromone addition), cells were registered over 10-min periods. Again, we observed that control cells had very low fluorescence and that a few cells exhibited transient increases in the fluorescence signal. We also observed that those cells that were imaged within the first 30 min of α-factor treatment exhibited low fluorescence levels, which was consistent with the previously reported 40-min lag before $[Ca^{2+}]_{cyt}$ increase. In contrast, movies taken after 30 min of α-factor treatment revealed very active $[Ca^{2+}]_{cyt}$ dynamics: yeast cells underwent fast and transient increases, or bursts, of $[Ca^{2+}]_{cyt}$ (Figure 2A). Data analysis showed that pheromone-induced $[Ca^{2+}]_{cyt}$ bursts are heterogeneous and sometimes overlapping and have different morphologies and lifespans (Figure 2, A and B). Most bursts have lifespans <30 s (70% of 90 registered bursts) and exhibit abrupt increase, reaching maximum levels in <4s (Figure 2, B and C). We also observed that the majority of $[Ca^{2+}]_{cyt}$ bursts (70% of 225 registered bursts) exhibit a decay behavior that fits with a single-exponential function (Supplemental Figure S1). Because the decay times derived from these fits are more than one order of magnitude larger than the reported unbinding time of Ca^{2+} from GcaMP6f (Chen *et al.*, 2013), we propose that the observed fluorescence
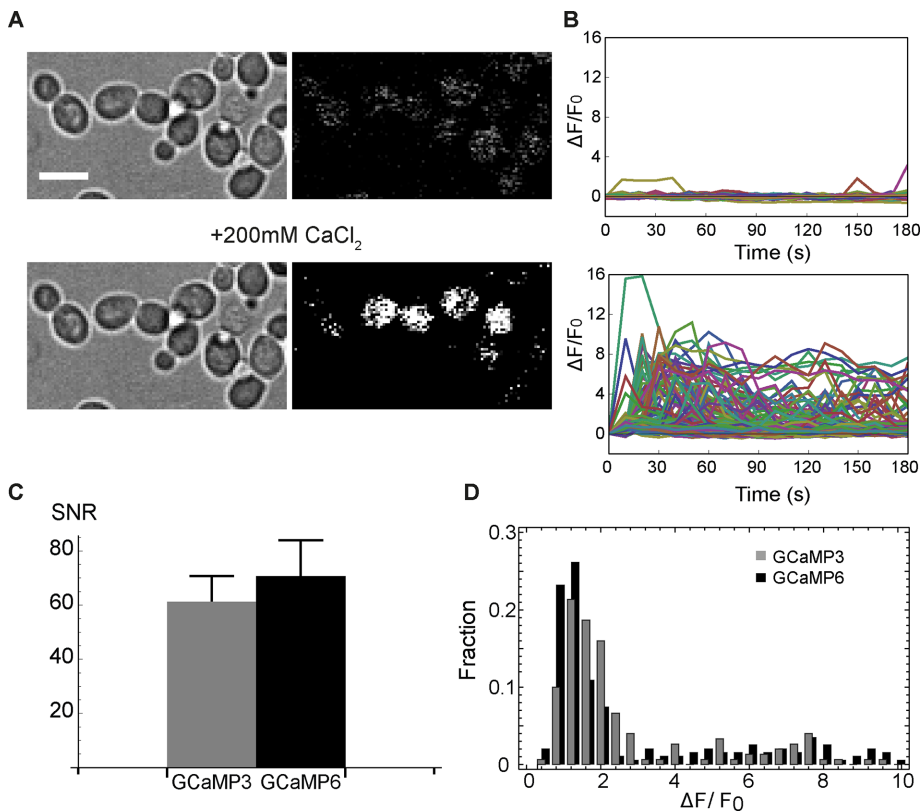
FIGURE 1: GCaMP sensor performance during yeast response to calcium stress. (A) GCaMP6f-expressing yeast cells were cultured up to mid log phase, attached to glass-bottom dishes, and then treated with 200 mM $CaCl_2$. Bar, 5 μm. (B) Normalized fluorescence (F/F_0) traces of single cells before (top) and after (bottom) addition of 200 mM $CaCl_2$. Each cell is represented by a different color; 185 (top) and 208 (bottom) cell traces for each condition. (C) Comparison of mean SNR of response of both GCaMP indicators in calcium-stressed cells. SNR was computed as the ratio between the maximal fluorescence response amplitude (F/F_0) and the SD of the basal fluorescence trace of nonstressed cells. (D) Normalized distributions of maximum F/F_0 values registered in 151 and 206 cells with GCaMP3 and GCaMP6f, respectively; bin size, 0.4. See *Materials and Methods* for image analysis and F/F_0 signal quantification.

changes in $[Ca^{2+}]_{cyt}$. The remaining 60% of cells experienced at least one burst during the 100-min registration (Figure 3A). This raised the question of whether $[Ca^{2+}]_{cyt}$ bursts were characteristic of a specific phase of the cell cycle. Morphological categorization of cells at the moment of burst occurrence indicated that mitotically active yeast cells experience bursts at any point of their cell cycle. However, when we quantified the number of bursts per cell cycle phase and compared the resulting distribution with the average time the monitored cells invest in each phase, we realized that G1 phase bursts were clearly overrepresented (Figure 3B). A more detailed probabilistic analysis indicated that this observed bias cannot be accounted for by a model in which calcium bursts occur at equal rates regardless of the cell phase and that they preferentially arise when cells are transitioning either G1 or S phase (*Materials and Methods*).

Burst morphologies of mitotically active cells were characterized by low amplitudes ($\Delta F/F_0 \leq 1$ in 92% of total burst population; Supplemental Figure S3) and short lifespans (<20 s in 87% of total burst population; Supplemental Figure S3). These results indicated that although $[Ca^{2+}]_{cyt}$ is maintained at low levels during normal cell growth in standard conditions, there are discrete $[Ca^{2+}]_{cyt}$ bursts during the cell cycle. These observed bursts might be implicated in fine-tuning of different cell cycle regulators that are CN effectors, such as Hcm1 (Arsenault *et al.*, 2015), Elm1 (Goldman *et al.*, 2014), and Rga2 (Ly and Cyert, unpublished data). [AQ 2]

decays faithfully reflect the underlying reduction of the free cytosolic Ca^{2+} concentration. Thus the observed single-exponential decay suggests that the cytosolic calcium concentrations reached during the pheromone response do not saturate the prevalent cytosolic calcium–removing systems.

Mitotically active yeast cells experience low frequency of $[Ca^{2+}]_{cyt}$ bursts

We next addressed how mitotically active cells experience $[Ca^{2+}]_{cyt}$ dynamics and how the dose of pheromone affects this during cell growth polarization. For this, we cultured *MAT*a GCaMP6f *bar1*Δ cells to mid log phase, treated them with different concentrations of α-factor, and then monitored them over 100 min. We chose this imaging range because, in our experimental conditions, it was long enough to accommodate a whole cell cycle in nontreated cells and shmoo formation in pheromone-treated cells (Supplemental Movie S2). Because we did not detect $[Ca^{2+}]_{cyt}$ bursts with lifespans <7 s (Figure 2B), we used a 0.4 frame/s sampling rate to avoid phototoxicity without losing signal detection capacity. We quantified two basic features of $[Ca^{2+}]_{cyt}$ bursts—amplitude ($\Delta F/F_0$) and duration—and also monitored the number of bursts per cell over 100 min (frequency; Figure 3). We found that 40% of mitotically active cells transit a complete cell cycle without experiencing noticeable

Mating pheromone concentration modulates the frequency of $[Ca^{2+}]_{cyt}$ bursts

In pheromone-treated cells, we observed that an α-factor concentration as low as 1 nM triggers a small but noticeable increase in $[Ca^{2+}]_{cyt}$ burst frequency, whereas an intermediate dose (5 nM), near the α-factor receptor Ste2 dissociation constant, is sufficient to produce a fivefold increase in the average number of burst occurrences (Figure 3C). High pheromone concentrations (10, 100 nM) elicit a maximum response in which 88% of the cells undergo between 5 and 15 bursts. Within the registered time frame (100 min), we did not find a periodic occurrence of bursts, but we did observe a lag phase (see later discussion). Unlike this clear increase in frequency, $[Ca^{2+}]_{cyt}$ burst morphologies suffered minor changes all over the dose–response curve. Burst amplitude distributions moved toward higher values with α-factor addition. For example, 23% of bursts in nontreated cells had $\Delta F/F_0 > 1$, whereas this percentage increased to 40% in 100 nM α-factor–treated cells (Supplemental Figure S3). Similarly, α-factor addition triggered the appearance of more bursts with longer lifespans: whereas 26% of bursts in nontreated cells lasted >20 s, in 100 nM α-factor–treated cells, this proportion rose to 45% (Supplemental Figure S3). However, for both parameters, we did not observe a clear dose–response behavior as we did for burst frequencies (compare insets in Figure 3C and Supplemental
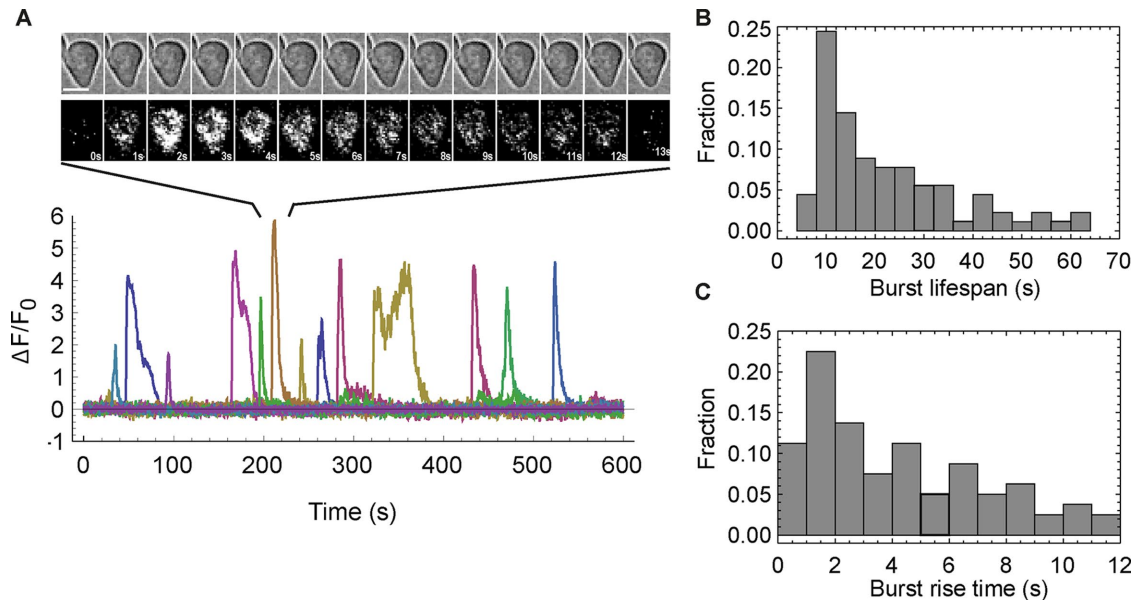
FIGURE 2: Pheromone-induced $[Ca^{2+}]_{cyt}$ bursts are heterogeneous. *MAT**a*** GCaMP6f cells were grown to mid log phase, treated with 6 μM α-factor during 30–45 min, and then registered over 10-min periods at 5 frames/s. (A) Examples of F/F_0 traces of different yeast cells responding to α-factor. Each color represents a single cell. The film strip shows an example of a polarized cell experiencing a 12-s $[Ca^{2+}]_{cyt}$ burst. Bar, 5 μm. Normalized distributions of $[Ca^{2+}]_{cyt}$ burst life spans (B) and rise times (C); 90 $[Ca^{2+}]_{cyt}$ bursts from 90 different pheromone-responding cells registered in four independent experiments. Bin sizes are 4 and 1 s for B and C, respectively.

Figure S3). Integration of $[Ca^{2+}]_{cyt}$ traces of 100 nM α-factor–treated cells confirmed our observations of a 30-min lag phase before burst frequency increase (Figure 3D) and are consistent with bulk measurements using radioactive calcium or aequorin (Ohsumi and Anraku, 1985; Muller *et al.*, 2001). In accordance with those authors' observations, we found that $[Ca^{2+}]_{cyt}$ burst frequency increase is coincident with shmoo formation active growth polarization at all α-factor concentrations tested (Figure 3D).

Frequency modulation (FM) of Ca^{2+} bursts is widely used by mammalian cells to encode different input signals, which are then decoded by signaling molecules and transcription factors to execute appropriate cellular responses (Dolmetsch *et al.*, 1998; Kupzig *et al.*, 2005; Thurley *et al.*, 2014). The α-factor–burst frequency dose–response curve (Figure 3C, inset) matches the equilibrium binding curve of α-factor to Ste2 and the α-factor–transcriptional induction dose–response curve, indicative of the phenomenon known as dose–response alignment, common to many other signaling systems (Yi *et al.*, 2003; Colman-Lerner *et al.*, 2005). FM of intracellular signals has been reported in budding yeast, in which different stresses modulate the frequency of nuclear translocation of transcription factors Msn2 (Jacquet *et al.*, 2003; Petrenko *et al.*, 2013; Lin *et al.*, 2015), Mig1 (Lin *et al.*, 2015), and CN-responsive Crz1 (Cai *et al.*, 2008). Remarkably, we observed that during the pheromone response, Crz1 exhibits bursts of nuclear localization (Supplemental Figure S3). We do not know whether these observed Crz1 bursts correlate with $[Ca^{2+}]_{cyt}$ bursts.

In the absence of stress, Crz1 locates in the cytosol, but high extracellular Ca^{2+} stress triggers a series of unsynchronized Crz1 nuclear localization bursts (Cai *et al.*, 2008). Extracellular Ca^{2+} concentration modulates the frequency of Crz1 nuclear localization bursts, which, in turn, promote transcriptional bursts of Crz1-dependent downstream genes. FM of Crz1 nuclear localization enables coordinated control of multiple target genes, keeping their relative expression constant over a wide dynamic range of stressor input

(Cai *et al.*, 2008). A similar scenario is proposed for stress-induced Msn2 nuclear localization bursts, for which FM elicits a more robust transcriptional response than does amplitude modulation (Hao and O'Shea, 2012; Petrenko *et al.*, 2013). It is assumed that during mating, the strength of pheromone signaling increases up to the culminating point of cell–cell fusion (Brizzio *et al.*, 1996). Thus, as mating progresses, frequency-modulated regulation of Ca^{2+} bursts might result in coordinated control of Ca^{2+} effectors in both partners. Yeast cells down-regulate the pheromone signal over time, resuming mitotic growth when a partner is not found, even in the presence of pheromone (Moore, 1984). Multiple negative feedback mechanisms prevent sustained pheromone activation because it causes cell death (Zhang *et al.*, 2006). The Ca^{2+}/CN signaling down-regulates the pheromone response by inhibiting Ste12-dependent gene expression and promoting internalization of the α-factor receptor Ste2 (Cyert *et al.*, 1991; Alvaro *et al.*, 2014; Goldman *et al.*, 2014). Cyert and Ly (unpublished data) found that at high pheromone concentra- [AQ 3] tions, CN dephosphorylates Rga2, leading to Cdc42 signaling reduction and pheromone response down-regulation. Thus pheromone-induced modification of Ca^{2+} burst frequencies might help yeast cells to evaluate and decide whether to quit or pursue the mating program.

Both HACS and LACS are involved in frequency modulation of pheromone-induced $[Ca^{2+}]_{cyt}$ bursts

We next asked how the known calcium import systems HACS and LACS affect amplitude, duration, and frequency of pheromone-induced $[Ca^{2+}]_{cyt}$ bursts. We observed that in the absence of extracellular calcium, pheromone treatment is unable to induce an increase in $[Ca^{2+}]_{cyt}$ burst frequency (Supplemental Figure S3), indicating that this response is mainly caused by extracellular calcium import and not by release from intracellular stores. To address this question, we monitored *MAT**a*** mutant cells impaired for HACS (*mid1Δ*), LACS (*fig1Δ*), or both (*mid1Δ fig1Δ*). $[Ca^{2+}]_{cyt}$ traces of mitotically active
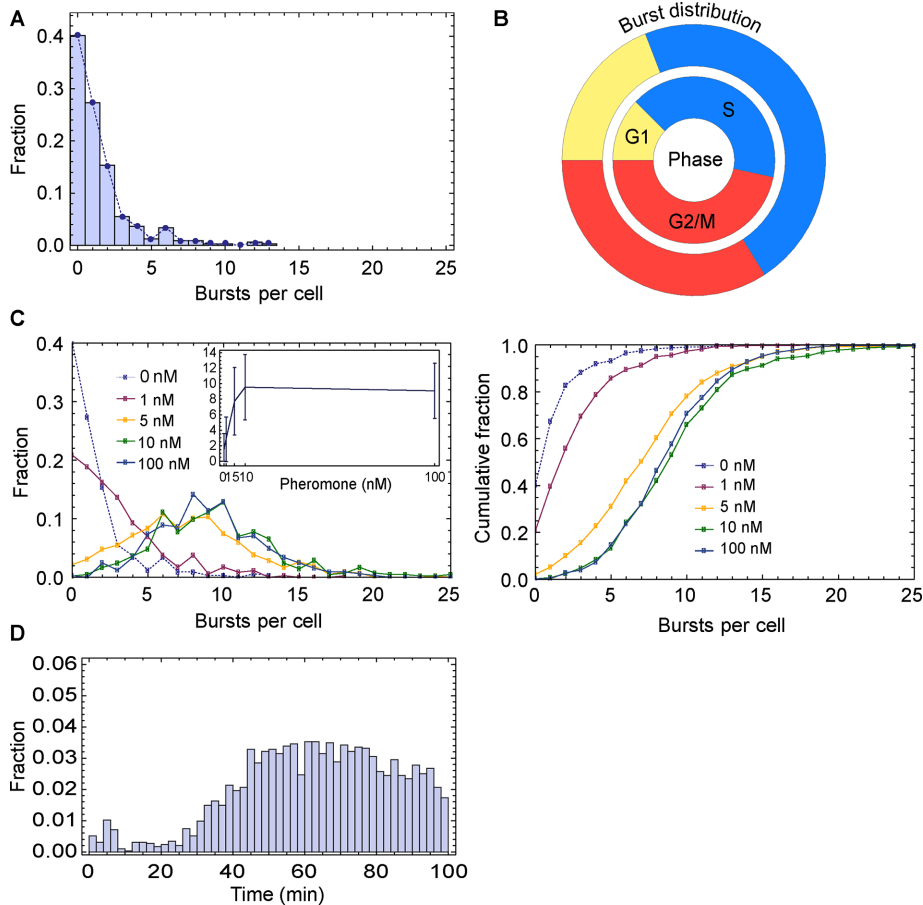
FIGURE 3: Calcium burst occurrences in mitotically active and pheromone-responsive cells. (A) *MAT**a*** GCaMP6f cells were cultured up to early log phase (OD$_{600nm}$ = 0.2) in SD medium and then imaged over 100 min. The F/F_0 traces were extracted, and the number of calcium bursts per cell was calculated (left). (B) To calculate the probability per unit time that a burst occurs while the cell is at a given phase, registered cells were first characterized morphologically, and then the average time distributions of G1, S, and G2/M phases (inner circle) and the burst distributions with respect to each phase (outer circle) were calculated. For both inner and outer circles, each phase area is proportional to the average time and burst distribution, respectively. Newly born cells, which have a longer G1 phase than mother cells, were excluded from this analysis. The mean fractions of time each cell spent in the G1, S, and G2/M phases during one cell cycle were 0.122, 0.408, and 0.470, respectively. The mean fractions of bursts that occurred while the cells were in the G1, S, and G2/M phases were 0.173, 0.464, and 0.363, respectively. The probabilities of burst occurrence per unit time computed as explained in *Materials and Methods* were 0.0288, 0.0234, and 0.0156 min^{-1} for G1, S, and G2/M phases, respectively. A total of 114 cells from three independent experiments were analyzed. (C) α-Factor increases calcium burst occurrence in a doses-dependent manner. *MAT**a*** GCaMP6f *bar1*Δ cells were grown to mid log phase, treated with 0, 1, 5, 10, and 100 nM α-factor (t = 0), and then imaged over 100 min. Density distributions of number of calcium bursts per cell. Inset, mean values vs. α-factor concentration. Error bars denote SDs. Right, cumulative distributions shown on the left. (D) Normalized distribution of number of bursts that occur in the whole cell population on 100 nM α-factor treatment of *MAT**a*** GCaMP6f *bar1*Δ cells. Data collected from three independent experiments with at least 300 registered cells per condition.

mutant cells exhibited no differences from those of wild type growing in the same conditions: most cells remained with low basal levels of GCaMP6f fluorescence and exhibited few low-amplitude bursts (Figure 4, Supplemental Figure S4, and Supplemental Table S5). On α-factor treatment, however, the three mutants exhibited a statistically significant increase in [Ca^{2+}]$_{cyt}$ burst frequency (Figure 4, A–C, and Supplemental Table S5) but a very limited one compared with wild-type cells (Figure 4D). These results indicate that in response to pheromone, both influx systems are active. Moreover, analyzing the

cumulative distributions of [Ca^{2+}]$_{cyt}$ burst frequencies, we found no differences between single and double mutants, suggesting that in our tested conditions, HACS and LACS function nonadditively (Figure 4D and Supplemental Table S5). The fact that the *mid1*Δ *fig1*Δ double mutant is able to increase [Ca^{2+}]$_{cyt}$ burst frequency also suggests that either there is a third import system, like the proposed glucose-induced calcium flux system (Groppi *et al.*, 2011), or there is a compensatory release from internal calcium stores. How does pheromone response trigger [Ca^{2+}]$_{cyt}$ bursts? Although the mechanisms of HACS or LACS activation have not been defined, it has been suggested that Cch1 is a mechanosensitive channel (Kanzaki *et al.*, 1999). Thus cell growth polarization and subsequent plasma membrane stretch may activate Cch1.

Statistical analysis of the cumulative distributions of [Ca^{2+}]$_{cyt}$ burst amplitudes and lifespans showed that in both tested conditions, *mid1*Δ cells underwent bursts with higher amplitudes than did wild-type, *fig1*Δ, and *fig1*Δ*mid1*Δ cells (Figure 5, A and B, and Supplemental Table S5). In contrast, lower amplitudes characterized *fig1*Δ cell bursts in the absence of pheromone (Figure 5B). Like *mid1*Δ cells, *fig1*Δ *mid1*Δ double mutants showed bursts but with higher amplitudes in response to pheromone (Figure 5A). Although burst lifespans seem to be different for vegetative growing *fig1*Δ and *mid1*Δ cells (Figure 5D), the Kolmogorov–Smirnov (KS) test does not reject the hypothesis that lifespans of all strains belong to the same distribution (Supplemental Table S5). On pheromone treatment, *mid1*Δ cells showed bursts with higher lifespans, whereas no differences were detected for the other three strains according to the KS test (Figure 5C and Supplemental Table S5). In short, these results indicated that HACS-impaired cells (*mid1*Δ) experienced bursts with higher amplitudes and lifespans in response to α-factor. Of interest, whereas Fig1 localizes at the shmoo tip during growth polarization, Cch1 is broadly distributed throughout the plasma membrane and is excluded from the shmoo tip (Yoshimura *et al.*, 2004; Aguilar *et al.*, 2007). Therefore it is expected that LACS- and HACS-mediated Ca^{2+} entries are spatially segregated, perhaps reflecting signaling over different subsets of Ca^{2+} effectors.

Live monitoring of [Ca^{2+}]$_{cyt}$ in fungi at the single-cell level has been hampered by the lack of sensitive, stable, and high-SNR sensors. Our results indicate that GCaMP sensors can be used to obtain detailed information on Ca^{2+} dynamics in *S. cerevisiae*. GCaMP sensors are being used in filamentous fungi (Nick Read, personal communication), where it is well established that Ca^{2+} signaling is required for hyphal growth and pathogenicity
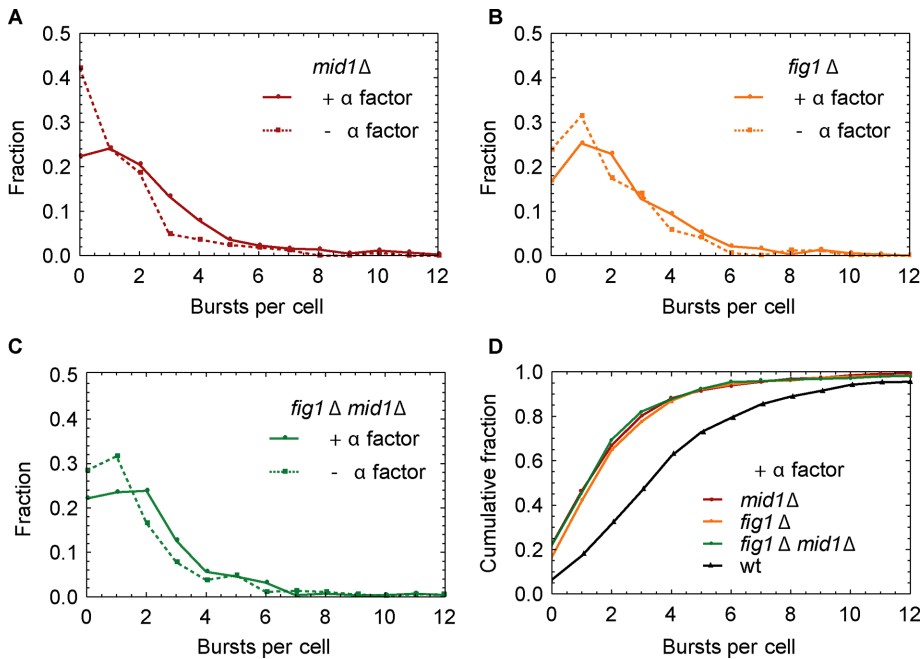
FIGURE 4: Both HACS- and LACS-impaired cells are still able to increase α-factor–dependent [Ca^{2+}]$_{cyt}$ burst frequencies. Normalized distributions of the number of bursts in *mid1Δ* (A), *fig1Δ* (B), and *fig1Δ mid1Δ* (C) cells with and without α-factor. (D) Corresponding cumulative distributions of burst occurrences in α-factor–treated cells. Normalized distributions were obtained from plots of at least 200 different cells (per strain and condition) in three independent experiments.
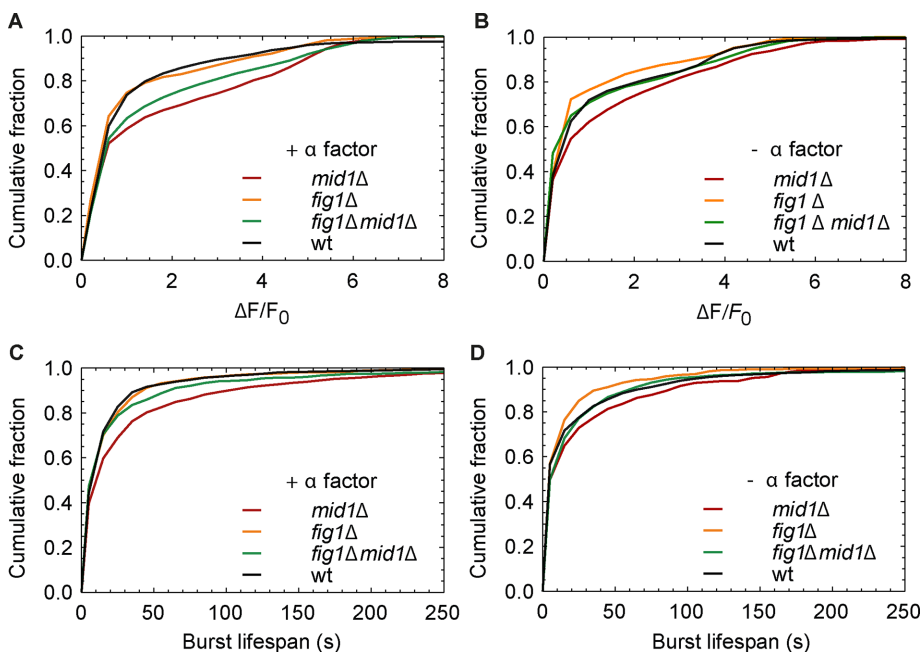

FIGURE 5: [Ca^{2+}]$_{cyt}$ bursts in *mid1Δ* cells have greater amplitudes and life spans. Cumulative distributions of burst amplitudes (A, B) and lifespans (C, D) in wild-type, *mid1Δ*, *fig1Δ*, and *mid1Δ fig1Δ* strain cells in the presence (A, C) or absence (B, D) of α-factor. Density distributions were obtained from traces of at least 200 different cells (per strain and condition) in three independent experiments.

(Munoz *et al.*, 2015). In *Candida albicans*, Ca^{2+} uptake is required for tropic growth of hyphae (Brand *et al.*, 2007). It has been suggested that localized Ca^{2+} uptake may provide positional information needed to define the site for polarized growth via a

mechanism that requires Cch1, Cdc42, and its guanine exchange factor, Cdc24 (Brand *et al.*, 2014). Monitoring Ca^{2+} dynamics in single cells might reveal the presence of cytosolic Ca^{2+} gradients in different fungi species and their relevance for normal and pathogenic physiology.

MATERIALS AND METHODS
GCaMP expression vector construction
GPD1 promoter was obtained from PYM-N14 (Janke *et al.*, 2004) and amplified by PCR using primers BamH1GPDp-F (CGT AGG ATC CGA GCT CAG TTT ATC ATT) and Xho1GPDp-R (GTC ACT CGA GTC TAG AAT CCG TCG AAA) adding *Bam*HI and *Xho*I sites and cloned into plasmid pRS306N from the EUROSCARF collection (Taxis and Knop, 2006). This plasmid was digested with *Sac*I, and the 988–base pair fragment containing *GPD1*-promoter followed by *ADH1*-terminator was ligated into *Sac*I-digested pRS306K, an integrative *S. cerevisiae* plasmid, at *URA3* loci with the dominant marker *kanMX4* (Taxis and Knop, 2006). The resulting vector was called pRS306K-GPD1p-ADH1t-a.

GCaMP3 and GCaMP6f coding sequences
To generate the final vector, pCMV-GCaMP3 and pCMV-GCaMP6f mammalian expression vectors obtained from AddGene (Cambridge MA) were used as templates to perform RFcloning reactions (van den Ent and Lowe, 2006) designed to precisely insert GCaMP3 or GCaMP6f open reading frames in GPD1p-ADH1t in the yeast integrative vector pRS306K-GPD1p-ADH1t-a. These final vectors were verified by sequencing and subsequently linearized for yeast transformation. The Crz1-GFP tagging strain was generated by PCR and homologous recombination using the plasmid pFA6a-link-yEGFP-CaURA3 (Sheff and Thorn, 2004).

Yeast strains and growth conditions
A complete list of strains used in each experiment is given in Supplemental Table S5. All strains were in the W303 background (leu2-3, 112 trp1-1 can1-100 ura3-1 ade2-1 his3-11, 15). Cells were grown in either rich medium YPD (1% yeast extract, 2% Bacto-peptone, and 2% glucose) or synthetic defined medium (SD) containing 0.67% yeast nitrogen base without amino acids (YNB; Difco), 2% glucose, and the appropriate drop-out mixture of amino acids according to supplier's instructions (CSM; Sunrise Science Products, San Diego, CA). Synthetic growth media lacking calcium were prepared similarly using calcium-free yeast nitrogen base reagents (YNB-CaCl2; Sunrise Science Products). In general, yeast strains were grown in 10 ml of

rich medium YPD to an $OD_{600} = 0.8$–1. For all microscopy experiments, yeast cells were cultured for a minimum of 18 h in SD and supplemented with 80 ng/ml adenine (Sigma- Aldrich, St. Louis, MO) at 30°C to OD = 0.2–0.4. For imaging, 200 μl of cell culture was incubated in concanavalin-A (Sigma-Aldrich)–coated chambers for 10 min (#1.5 glass; MatTek, Ashland, MA). Finally, SD medium was replaced by a fresh one, and cells were imaged. For calcium-free treatments, cells were grown overnight in SD and then transferred to chambers and washed three times with SD-Ca^{2+} before use. The α-factor mating pheromone was obtained from Sigma-Aldrich.

Microscopy setting

Time-lapse imaging was performed on a Leica DMI6000,TCS-SP5 with a resonant scanner (8000-Hz scanning frequency) using an HCX PL APO 63/1.4-060 CS oil objective and equipped with an automatically programmable XY stage (Mark & Find; Leica) in an environment chamber preequilibrated to 30°C. Images were acquired using an argon ion laser at wavelength of 488 nm with 30% laser power, a pinhole set to 3 airy units, photomultiplier tube range of 495–589 nm, 784 gain, and –0.2 offset. Image formats of 512 × 512– and 282 × 282–nm pixel size were used for all acquired movies. For calcium stress, the sampling rate was 1 frame/10 s. For high-speed imaging of pheromone-treated cells, it was 5 frames/s, and for long-term monitoring, it was 0.4 frames/s. Measurements of mitotic cell growth and cell growth polarization during the pheromone response indicated that all defined imaging conditions were innocuous for both processes (unpublished data).

Image analysis. I. Obtaining a reporter of changes in [Ca^{2+}] that can be compared across cells

For short-term (10–13 min) movies, cells were manually segmented. For long-term (100 min) movies, single cells were automatically segmented from transmitted light images using CellStat (Kvarnstrom et al., 2008). For mitotically active cell analysis, cells were randomly selected using CellStat, and only those cells that were segmented throughout the whole time lapse were kept for further analysis. Because we used asynchronous cultures, for α-factor treatment experiments, after CellStat segmentation, we selected cells that at $t = 0$ were morphologically compatible with G_1 phase (unbudded cells). In all cases, we excluded from further analysis selected cells that evidenced loss of integrity upon movie inspection.

Connected regions on the image $A_l(t_k)$ corresponding to single cells (each one identified by the subscript l) were determined as a function of time t_k using segmented images.

We computed the normalized calcium signal for each cell i at time t_k as

$$F_l(t_k) = \frac{1}{N_p(A_l(t_k))} \sum_{(x_i, y_j) \in A_l(t_k)} g(x_i, y_j, t_k) \tag{1}$$

where $g(x_i, y_j, t_k)$ is the registered fluorescence at time t_k from the pixels located at (x_i, y_j) and $N_p(A_l(t_k))$ is the number of pixels in the region $A_l(t_k)$ of the image associated with the l th cell at time t_k. We computed the background noise for each cell $BG_k(t_k)$ as

$$BG_l(t_k) = \frac{1}{N_p^*(A_l^*(t_k))} \sum_{(x_i, y_j) \in A_l^*(t_k)} g(x_i, y_j, t_k) \tag{2}$$

where $A_p^*(t_k)$ is an empty region contiguous to the analyzed cell. The number of pixels $IN_p^*(A_i^*(t_k))$ is similar to the number of pixels of $N_p(A_l(t_k))$. We then subtracted the background noise $BG_k(t_k)$ from the normalized fluorescence to define

$$h_l(t_k) = F_l(t_k) - BG_l(t_k) \tag{3}$$

To correct for photobleaching, we took the sequence for each cell $\{h_l(t_k)\}_{t_k=0}^{T}$, with T the duration of the experiment, and extracted from it the values $h_l(t_k)$ associated with easily recognizable fluorescence bursts. We then fitted this pruned sequence $\{h_l(t_k)\}_{t_k=0}^{T}$ by an exponential:

$$f_{b,l}(t_k^*) = C_l e^{-\lambda_l t_k^*} \tag{4}$$

Finally, we defined a corrected expression for photobleaching-normalized fluorescence as

$$f_l(t_k) = \frac{h_l(t_k)}{f_{b,l}(t_k^*)} \tag{5}$$

To account for differences in GCaMP expression or cell size between cells, which result in different fluorescence basal levels, we computed the basal level associated with each cell as

$$f_{0l} = \frac{1}{N^*} \sum_{t_k^*} h_l(t_k^*) \tag{6}$$

where N^* is the total number of t_k^* times of the sequence without easily recognizable fluorescence bursts. We finally computed the increase in the corrected-for-photobleaching normalized fluorescence for each cell as a function of time as

$$\left.\frac{\Delta F}{F_0}\right|_l (t_k) = \frac{f_l(t_k) - f_{0l}}{f_{0l}} \tag{7}$$

We assumed that this quantity was a good reporter of the changes in cytoplasmic Ca^{2+} and can be compared between cells despite their differences in dye load or size. It is thus the quantity that we used for the analysis.

Image analysis. II. Identification of Ca^{2+} bursts

To set a criterion that distinguishes Ca^{2+} bursts from spurious (random) changes in basal fluorescence, we applied the following iterative procedure. The procedure first takes, for each cell l, the pruned sequence $\Delta F / F_0|_l (t_k^*)$ with the times t_k^* as defined before. It then computes for each time t_k^* of the sequence the mean $\mu_{i,l}$ and SD $\sigma_{i,l}$ of $\Delta F / F_0|_l (t_k^*)$ over the 250 times t_k^* preceding t_i^*:

$$\mu_{i,l} = \frac{1}{250} \sum_{t_k^* < t_i^*} \left.\frac{\Delta F}{F_0}\right|_l (t_k) \tag{8}$$

$$\sigma_{i,l} = \frac{1}{250} \sum_{t_k^* < t_i^*} \left(\left.\frac{\Delta F}{F_0}\right|_l (t_k) - \mu_{i,l}\right)^2 \tag{9}$$

From the element 251 to t_i^*, the protocol sweeps over the 250 elements of the sequence before t_i^* and computes $\left|\Delta F / F_0|_l (t_k^*) - \mu_{i,l}\right| / \sigma_{i,l}$. If this ratio is >3 for some t_k^*, the corresponding element $\Delta F / F_0|_l (t_k^*)$ is excluded from the pruned sequence. The newly excluded time is included in a new set, t_{brust}. The procedure is repeated, iteratively sweeping back and forth (using the 250 times that follow t_i^*) in time until no more elements departing from the mean by >3 SDs are found. The sweepback classifies the first 250 elements of the principal of the sequence. The procedure is applied subsequently to all the times t_i^* in the latest pruned sequence. Finally, we look for sets of at least three consecutive times t_k^* in t_{brust} and associate the corresponding elements $\Delta F / F_0|_l (t_k^*)$ with a Ca^{2+} burst.

Computation of probabilities of cell cycle burst occurrence

Because newly born cells spend more time in G1 phase than mother cells and because complete registration of cell cycles of mother cells was more frequent in our 100-min time-lapse movies, we restricted this analysis to mother cells (114 cells over three independent experiments) that experienced one or more Ca^{2+} bursts. To check how meaningful it was to pool the data from the three experiments together, we compared the distributions of phase duration obtained for each experiment. A KS test did not reject the hypothesis that the data from any two of the experiments were drawn from the same distribution (confidence level of 0.05). Therefore we decided to pool the data coming from the 114 cells together. In principle, calcium bursts can occur at any time along each cell phase. Thus, to distinguish situations with different numbers of bursts during the time course of one cycle, we calculated probability densities per unit time. To this end, we coarse-grained the data set using the time duration dt of the longest typical Ca^{2+} burst (~22 s). This duration was much smaller than the mean times of ~500, 1750, and 2000 s that each cell invests in each the three phases that we considered for the analysis—G1, S, and G2/M, respectively; it was also much smaller than the mean interburst time interval (~2050 s). We then looked at the time course of the fluorescence, $\Delta F/F_0(t)$, of each selected cell and assigned a 1 or a 0, respectively, to each time interval of duration dt if $\Delta F/F_0(t)$ either showed or did not show a burst in the corresponding time interval. Given the relationship between dt and the mean interburst time, we expected each interval of size dt to contain at most one burst. It may occur that a burst starts during a particular interval and ends during the following one. In such cases, we assigned a 1 to the interval that contained most of the burst duration and a 0 to the other one. If the burst was equally distributed between the two consecutive intervals, we assigned the 1 to either one of them at random. In this way, we digitized the data set, and the computation of the probability of burst occurrence was simply done by counting bursts (i.e., differences in burst duration were not considered for the computation). Thus we calculated the probability that a burst occurs during any time interval of duration dt as

$$P_b = \frac{N_b}{N_c T / dt} = \frac{N_b}{N_c} \frac{dt}{T} \tag{10}$$

where T is the duration of the experiment, N_c is the number of analyzed cells (mothers with at least one Ca^{2+} burst that are visualized during the whole experimental time course), and N_b is the total number of bursts displayed by the whole set of analyzed cells during the experiment.

In the same way that we assigned 0's and 1's to each analyzed cell at a particular time interval of duration dt, we assigned a symbol G_1, S, or G_2/M, depending on which of these three phases the cell was in. We identified each phase according to morphological characterization of transmitted-light time-lapse movies as follows: unbudded cells were categorized as G_1-phase cells. The S phase was defined as the lapse between the first evidence of a nascent bud and the point where the bud/mother cell diameter ratio was <0.5. The G_2/M phase was defined as the lapse between the end of S phase and the point where the common bud–mother cell longitudinal axis was broken, evidencing physical separation of daughters from mother cells. When any of these criteria was not easily distinguished, the cell was removed from the analysis. With the time points for each phase transition, we then computed the probability that a cell is at a given phase P_{ph} (ph = G_1, S, G_2/M) as the mean over all selected cells of the fraction of time each selected cell spends at the given phase:

$$P_{ph} = \sum_{l=1}^{N_c} \frac{N_{ph,l}}{N_c} \frac{dt}{T}, \quad ph = G_1, S, G_2/M \tag{11}$$

where the subscript l identifies any of the N_c analyzed cells and $N_{ph,\,l}$ is the number of time intervals of duration dt during which the l th cell remains in the phase ph. We assumed that P_{ph} is also the (mean) fraction of time a cell spends at phase ph during each cell cycle:

$$P_{ph} = \frac{\lambda_{ph}}{\lambda} \tag{12}$$

where λ_{ph} is the mean duration of phase ph during a cell cycle and λ is the mean cell cycle duration. We computed the duration of each phase for each cell following each selected cell during one cycle. We then computed λ_{ph} as the mean over these phase durations. We computed the joint probability that, during a time interval of duration dt a cell is at a given phase and displays a burst as

$$P(ph \& b) = \sum_{l=1}^{N_c} \frac{N_{b,ph,l}}{N_c} \frac{dt}{T} \tag{13}$$

where $N_{b,\,ph,\,l}$ is the total number of burst displayed by the l th cell while being at the phase ph. Clearly, the total number of bursts displayed by the l th cell, $N_{b,\,l}$, satisfies

$$N_{b,l} = \sum_{ph} N_{b,ph,l} \tag{14}$$

where the sum is performed over the three phases. We computed the conditional probability that a cell is at a given phase ph at a particular time interval of duration dt, given that at that time interval the cell displays a burst, as

$$P(ph|b) = \frac{P(ph \& b)}{P_b} = \sum_{l=1}^{N_c} \frac{N_{b,ph,l}}{N_b} \tag{15}$$

This is the quantity that we compared against P_{ph} in the text.

We computed the conditional probability that a cell has a burst during a time interval of duration dt, given that it is at a particular phase ph during that time interval, as

$$P(b|ph) = \frac{P(ph \& b)}{P_{ph}} = \frac{1}{P_{ph}} \sum_{l=1}^{N_c} \frac{N_{b,ph,l}}{N_c} \frac{dt}{T} = \frac{\sum_{l=1}^{N_c} N_{b,ph,l}}{\sum_{l=1}^{N_c} N_{ph,l}} \tag{16}$$

Now each cell l spends a total time $t_{ph,l}$ in each phase ph given by

$$t_{ph,l} = N_{ph,l} dt \tag{17}$$

during the time course of the experiment, so that, on average, the cell spends a time

$$t_{ph} = \frac{1}{N_c} \sum_{l=1}^{N_c} N_{ph,l} dt \tag{18}$$

in phase ph during the experiment. The duration of each of the three performed independent experiments was slightly larger than the mean cell cycle duration λ. Thus we relate the mean phase duration λ_{ph} with the mean time t_{ph} a cell spends in phase ph during the time course of the experiment by

$$\lambda_{ph} = \frac{t_{ph}}{T} \lambda = \frac{\lambda}{TN_c} \sum_{l=1}^{N_c} N_{ph,l} dt \tag{19}$$

Inserting this expression in Eq. (16), we obtain

$$P(b|\text{ph}) = dt \frac{\sum_{l=1}^{N_c} N_{b,\text{ph},l}\lambda}{TN_c\lambda_{\text{ph}}} \qquad (20)$$

Inserting Eq. (15) in Eq. (20), we obtain

$$P(b|\text{ph}) = dt \frac{N_b P(\text{ph}|b)\lambda}{TN_c\lambda_{\text{ph}}} \qquad (21)$$

from which we compute the probability per unit time that a burst occurs while the cell is at a given phase ph as

$$R(b|\text{ph}) = \frac{N_b P(\text{ph}|b)\lambda}{TN_c\lambda_{\text{ph}}} \qquad (22)$$

These are the rates that are reported in Figure 3A.

We tested whether the observed bias of burst occurrence was compatible with a model in which calcium bursts occur at equal rates regardless of the cell phase. For this, we performed a chi-square goodness-of-fit test, considering the null hypothesis that the mean number of bursts during a phase was solely proportional to the mean phase duration. Pooling the data from three independent experiments (total number of bursts, 168), a comparison with the mean number of bursts per phase observed experimentally gave a chi-square value (8.92) that allows us to reject the null hypothesis at the 0.02 significance level. We then conclude that calcium bursts occur at higher rates when cells are transitioning either the G1 or S phase.

ACKNOWLEDGMENTS

REFERENCES

Aguilar PS, Engel A, Walter P (2007). The plasma membrane proteins Prm1 and Fig1 ascertain fidelity of membrane fusion during yeast mating. Mol Biol Cell 18, 547–556.

Alvaro CG, O'Donnell AF, Prosser DC, Augustine AA, Goldman A, Brodsky JL, Cyert MS, Wendland B, Thorner J (2014). Specific alpha-arrestins negatively regulate Saccharomyces cerevisiae pheromone response by down-modulating the G-protein-coupled receptor Ste2. Mol Cell Biol 34, 2660–2681.

Arsenault HE, Roy J, Mapa CE, Cyert MS, Benanti JA (2015). Hcm1 integrates signals from Cdk1 and calcineurin to control cell proliferation. Mol Biol Cell 26, 3570–3577.

Batiza AF, Schulz T, Masson PH (1996). Yeast respond to hypotonic shock with a calcium pulse. J Biol Chem 271, 23357–23362.

Bonilla M, Nastase KK, Cunningham KW (2002). Essential role of calcineurin in response to endoplasmic reticulum stress. EMBO J 21, 2343–2353.

Brand A, Shanks S, Duncan VM, Yang M, Mackenzie K, Gow NA (2007). Hyphal orientation of Candida albicans is regulated by a calcium-dependent mechanism. Curr Biol 17, 347–352.

Brand AC, Morrison E, Milne S, Gonia S, Gale CA, Gow NA (2014). Cdc42 GTPase dynamics control directional growth responses. Proc Natl Acad Sci USA 111, 811–816.

Brizzio V, Gammie AE, Nijbroek G, Michaelis S, Rose MD (1996). Cell fusion during yeast mating requires high levels of a-factor mating pheromone. J Cell Biol 135, 1727–1739.

Cai L, Dalal CK, Elowitz MB (2008). Frequency-modulated nuclear localization bursts coordinate gene regulation. Nature 455, 485–490.

Chen TW, Wardill TJ, Sun Y, Pulver SR, Renninger SL, Baohan A, Schreiter ER, Kerr RA, Orger MB, Jayaraman V, et al. (2013). Ultrasensitive fluorescent proteins for imaging neuronal activity. Nature 499, 295–300.

Colman-Lerner A, Gordon A, Serra E, Chin T, Resnekov O, Endy D, Pesce CG, Brent R (2005). Regulated cell-to-cell variation in a cell-fate decision system. Nature 437, 699–706.

Cunningham KW (2011). Acidic calcium stores of Saccharomyces cerevisiae. Cell Calcium 50, 129–138.

Cyert MS, Kunisawa R, Kaim D, Thorner J (1991). Yeast has homologs (CNA1 and CNA2 gene products) of mammalian calcineurin, a calmodulin-regulated phosphoprotein phosphatase. Proc Natl Acad Sci USA 88, 7376–7380.

Cyert MS, Philpott CC (2013). Regulation of cation balance in Saccharomyces cerevisiae. Genetics 193, 677–713.

Denis V, Cyert MS (2002). Internal Ca(2+) release in yeast is triggered by hypertonic shock and mediated by a TRP channel homologue. J Cell Biol 156, 29–34.

Dolmetsch RE, Xu K, Lewis RS (1998). Calcium oscillations increase the efficiency and specificity of gene expression. Nature 392, 933–936.

Fischer M, Schnell N, Chattaway J, Davies P, Dixon G, Sanders D (1997). The Saccharomyces cerevisiae CCH1 gene is involved in calcium influx and mating. FEBS Lett 419, 259–262.

Goldman A, Roy J, Bodenmiller B, Wanka S, Landry CR, Aebersold R, Cyert MS (2014). The calcineurin signaling network evolves via conserved kinase-phosphatase modules that transcend substrate identity. Mol Cell 55, 422–435.

Groppi S, Belotti F, Brandao RL, Martegani E, Tisi R (2011). Glucose-induced calcium influx in budding yeast involves a novel calcium transport system and can activate calcineurin. Cell Calcium 49, 376–386.

Hao N, O'Shea EK (2012). Signal-dependent dynamics of transcription factor translocation controls gene expression. Nat Struct Mol Biol 19, 31–39.

Iida H, Nakamura H, Ono T, Okumura MS, Anraku Y (1994). MID1, a novel Saccharomyces cerevisiae gene encoding a plasma membrane protein, is required for Ca2+ influx and mating. Mol Cell Biol 14, 8259–8271.

Iida H, Yagawa Y, Anraku Y (1990). Essential role for induced Ca2+ influx followed by [Ca2+]i rise in maintaining viability of yeast cells late in the mating pheromone response pathway. A study of [Ca2+]i in single Saccharomyces cerevisiae cells with imaging of fura-2. J Biol Chem 265, 13391–13399.

Jacquet M, Renault G, Lallet S, De Mey J, Goldbeter A (2003). Oscillatory nucleocytoplasmic shuttling of the general stress response transcriptional activators Msn2 and Msn4 in Saccharomyces cerevisiae. J Cell Biol 161, 497–505.

Janke C, Magiera MM, Rathfelder N, Taxis C, Reber S, Maekawa H, Moreno-Borchart A, Doenges G, Schwob E, Schiebel E, Knop M (2004). A versatile toolbox for PCR-based tagging of yeast genes: new fluorescent proteins, more markers and promoter substitution cassettes. Yeast 21, 947–962.

Kanzaki M, Nagasawa M, Kojima I, Sato C, Naruse K, Sokabe M, Iida H (1999). Molecular identification of a eukaryotic, stretch-activated nonselective cation channel. Science 285, 882–886.

Kupzig S, Walker SA, Cullen PJ (2005). The frequencies of calcium oscillations are optimized for efficient calcium-mediated activation of Ras and the ERK/MAPK cascade. Proc Natl Acad Sci USA 102, 7577–7582.

Kvarnstrom M, Logg K, Diez A, Bodvard K, Kall M (2008). Image analysis algorithms for cell contour recognition in budding yeast. Opt Express 16, 12943–12957.

Lin Y, Sohn CH, Dalal CK, Cai L, Elowitz MB (2015). Combinatorial gene regulation by modulation of relative pulse timing. Nature 527, 54–58.

Locke EG, Bonilla M, Liang L, Takita Y, Cunningham KW (2000). A homolog of voltage-gated Ca(2+) channels stimulated by depletion of secretory Ca(2+) in yeast. Mol Cell Biol 20, 6686–6694.

Martin DC, Kim H, Mackin NA, Maldonado-Baez L, Evangelista CC Jr, Beaudry VG, Dudgeon DD, Naiman DQ, Erdman SE, Cunningham KW

(2011). New regulators of a high affinity Ca2+ influx system revealed through a genome-wide screen in yeast. J Biol Chem 286, 10744–10754.

Moore SA (1984). Yeast cells recover from mating pheromone alpha factor-induced division arrest by desensitization in the absence of alpha factor destruction. J Biol Chem 259, 1004–1010.

Muller EM, Locke EG, Cunningham KW (2001). Differential regulation of two Ca(2+) influx systems by pheromone signaling in Saccharomyces cerevisiae. Genetics 159, 1527–1538.

Muller EM, Mackin NA, Erdman SE, Cunningham KW (2003). Fig1p facilitates Ca2+ influx and cell fusion during mating of Saccharomyces cerevisiae. J Biol Chem 278, 38461–38469.

Munoz A, Bertuzzi M, Bettgenhaeuser J, Iakobachvili N, Bignell EM, Read ND (2015). Different stress-induced calcium signatures are reported by aequorin-mediated calcium measurements in living cells of aspergillus fumigatus. PLoS One 10, e0138008.

Nakajima-Shimada J, Iida H, Tsuji FI, Anraku Y (1991). Monitoring of intracellular calcium in Saccharomyces cerevisiae with an apoaequorin cDNA expression system. Proc Natl Acad Sci USA 88, 6878–6882.

Ohsumi Y, Anraku Y (1985). Specific induction of Ca2+ transport activity in MATa cells of Saccharomyces cerevisiae by a mating pheromone, alpha factor. J Biol Chem 260, 10482–10486.

Paidhungat M, Garrett S (1997). A homolog of mammalian, voltage-gated calcium channels mediates yeast pheromone-stimulated Ca2+ uptake and exacerbates the cdc1(Ts) growth defect. Mol Cell Biol 17, 6339–6347.

Petrenko N, Chereji RV, McClean MN, Morozov AV, Broach JR (2013). Noise and interlocking signaling pathways promote distinct transcription factor dynamics in response to different stresses. Mol Biol Cell 24, 2045–2057.

Sheff MA, Thorn KS (2004). Optimized cassettes for fluorescent protein tagging in Saccharomyces cerevisiae. Yeast 21, 661–670.

Stathopoulos AM, Cyert MS (1997). Calcineurin acts through the CRZ1/TCN1-encoded transcription factor to regulate gene expression in yeast. Genes Dev 11, 3432–3444.

Taxis C, Knop M (2006). System of centromeric, episomal, and integrative vectors based on drug resistance markers for Saccharomyces cerevisiae. Biotechniques 40, 73–78.

Thurley K, Tovey SC, Moenke G, Prince VL, Meena A, Thomas AP, Skupin A, Taylor CW, Falcke M (2014). Reliable encoding of stimulus intensities within random sequences of intracellular Ca2+ spikes. Sci Signal 7, ra59.

Tian L, Hires SA, Mao T, Huber D, Chiappe ME, Chalasani SH, Petreanu L, Akerboom J, McKinney SA, Schreiter ER, et al. (2009). Imaging neural activity in worms, flies and mice with improved GCaMP calcium indicators. Nat Methods 6, 875–881.

van den Ent F, Lowe J (2006). RF cloning: a restriction-free method for inserting target genes into plasmids. J Biochem Biophys Methods 67, 67–74.

Viladevall L, Serrano R, Ruiz A, Domenech G, Giraldo J, Barcelo A, Arino J (2004). Characterization of the calcium-mediated response to alkaline stress in Saccharomyces cerevisiae. J Biol Chem 279, 43614–43624.

Yi TM, Kitano H, Simon MI (2003). A quantitative characterization of the yeast heterotrimeric G protein cycle. Proc Natl Acad Sci USA 100, 10764–10769.

Yoshimura H, Tada T, Iida H (2004). Subcellular localization and oligomeric structure of the yeast putative stretch-activated Ca2+ channel component Mid1. Exp Cell Res 293, 185–195.

Zhang NN, Dudgeon DD, Paliwal S, Levchenko A, Grote E, Cunningham KW (2006). Multiple signaling pathways regulate yeast cell death during the response to mating pheromones. Mol Biol Cell 17, 3409–3422.

ETOC:

This first systematic characterization of single-cell Ca^{2+} dynamics in *Saccharomyces cerevisiae* adapts GCaMP sensors to budding yeast to show that the pheromone modulates the frequency of cytosolic Ca^{2+} bursts. The Ca^{2+}-responsive transcription factor Crz1 experiences nuclear localization bursts during the pheromone response.

Author Queries

[AQ 1]:   Please provide postal codes for all affiliations.
[AQ 2]:   Can Ly and Cyert, unpublished data, be updated?
[AQ 3]:   Can Cyert and Ly be updated?